Int. J. Electrochem. Sci., 17 **(2022)** Article Number: 22098, doi: 10.20964/2022.09.46

International Journal of
ELECTROCHEMICAL
SCIENCE
www.electrochemsci.org

One-step Electrodeposition of CuNi Bimetallic Nanocatalyst Anchored on Reduced Graphene Oxide Modified Glassy Carbon Electrode for Nonenzymatic Sensing of Glucose

Tong Yang, Yu Xie, Xinning Zhang, Ruike Guo, Xin Yang[*]

Key Laboratory of Research and Utilization of Ethnomedicinal Plant Resources of Hunan Province, Hunan Engineering Laboratory for Preparation Technology of Polyvinyl Alcohol Fiber Material, Huaihua University, Huaihua 418000, PR China.
[*]E-mail: 01yangxin@163.com

Received: 23 April 2022 / *Accepted:* 14 July 2022 / *Published:* 7 August 2022

The reliable detection of glucose is desirable for various applications. Herein, a nonenzymatic glucose electrochemical sensor based on copper (Cu)-nickel (Ni) bimetallic nanocatalyst anchored on reduced graphene oxide (rGO) modified glassy carbon electrode (GCE) was fabricated. The controllable and in-situ formation of rGO/Cu-Ni nanocomposites onto GCE was achieved via a one-step electrodeposition strategy. The chemical constituents, crystallization degrees, surface morphologies, and electrocatalytic features of nanocomposites were characterized with different techniques. The electrochemical sensor exhibited superior synergistic effects towards electrocatalytic oxidation of glucose in alkaline solution, and was applied to determine glucose in human serum sample with satisfactory results. The universal methodologies for hybrid nanocomposites preparation and electrochemical platforms fabrication can be exploited in other food or pharmaceutical analysis.

Keywords: Glucose; Bimetallic nanocatalyst; Nanomatrix; Synergistic effects; Electrodeposition; Nonenzymatic sensor

1. INTRODUCTION

The sensitive, convenient, economical, and reliable glucose detection methods has become increasingly important for medical diagnosis, food industry, chemistry, biotechnology, and environmental protection [1]. Several approaches including colorimetry, chemiluminescence, fluorescent spectroscopy, UV-Visible spectroscopy, surface-enhanced Raman scattering, gas chromatography-mass spectrometry, high-performance liquid chromatography, and electrochemical techniques have been exploited for proficient detection of glucose [2]. Among numerous types of methods, electrochemical sensing of glucose based on enzymatic and nonenzymatic sensors are widely

investigated and attracted much attention. In general, glucose oxidase (GOx) and glucose dehydrogenase (GDH) are commonly applied in enzymatic glucose sensors. The notable advantages of enzymatic sensors lie in their high selectivity and sensitivity. Unfortunately, several drawbacks are inevitable during the utilization of those enzymes: (i) the high production cost and tedious immobilization steps. (ii) the thermal/physical/chemical instability, easy deactivation, and poor reproducibility. (iii) the interferences from other electroactive molecules due to the high overpotentials during the oxidation of enzymatically generated H_2O_2 [3-5].

Hence, various nano/microstructured nonenzymatic electrochemical sensors based on transition metals, noble metals, and metal oxides for electrocatalytic oxidation of glucose have been actively developed to be alternatives. Among those nonenzymatic sensing materials, the noble metals and metal oxides-based catalysts are either high cost or poor electrical conductivity, which limit their widespread applications. As a consequence, many earth-abundant transition metals, especially copper (Cu) and nickel (Ni) were chosen as preferable sensing components with taking into account the fabrication cost, electrical conductivity, chemical stability, and electrocatalytic activity. For instance, several amperometric nonenzymatic glucose sensors based on Cu nanoparticles anchored on multiwalled carbon nanotubes (MWCNs), graphene (Gr), nitrogen-doped graphene (NGr), and laser-induced graphene (LIGr) were developed by Wu [6], Luo [7], Shabnam[8], and Zhang [9], respectively. Various nanohybrids consisting of Ni nanoparticles combined with MWCNs [10, 11], reduced graphene oxide (rGO) [12, 13], and Gr [14] were adopted in nonenzymatic sensing of glucose. Although nonenzymatic sensing performances can be ameliorated by using monometallic-based materials to some extent compared with enzymatic sensors, novel electrocatalysts with superior performances are still needed.

In general, there are two typical strategies have been explored to realize more efficient electrocatalysts [15-18]. On the one hand, introducing other metal elements into host materials to obtain bimetallic nanocatalysts. Therefore, synergistic effects for electrocatalytic of glucose can be achieved. On the other hand, adopting highly conductive nanostructured matrices to provide more specific surface area. Hence, the electro-active sites and electron transfer of nanocomposites can be promoted. Up to now, few hybrid nanocomposites based on Cu-Ni bimetallic nanocatalyst anchored on conductive nanostructured matrices by means of electrodeposition, solvothermal, and thermal annealing methods have been qualified for glucose sensing. For example, the sequential electrodeposition of Ni and Cu nanoparticles decorated MWCNTs film modified electrodes for sensitively nonenzymatic glucose detection were fabricated by Lin [19] and Ammara [20]. The Cu-Ni bimetallic catalysts supported by chemically grafted carboxylated and functionalized CNTs were prepared by electrochemical methods and used for glucose electrochemical sensors [21, 22]. Cu together with Ni nanoparticles dispersed on NGr, rGO, TiO_2 nanotubes array, and Gr were shown to be viable materials for nonenzymatic sensing of glucose [23-26]. Considering the attractively unique properties of rGO, Ni, and Cu candidates, we reasonably expect that the Cu-Ni bimetallic nanocatalyst anchored on rGO (referred to as rGO/Cu-Ni) can inherently provide superior electrochemical performances for glucose detection. Unfortunately, there are no routes concerning one-step electrodeposition of rGO/Cu-Ni nanocomposites modified electrodes for quantitative analysis of glucose up to now.

The reasons mentioned above combined with our engaged researches inspire us to utilize the

synergistic effects originated from rGO/Cu-Ni nanocomposites for nonenzymatic electrochemical detection of glucose. The controllable and in-situ formation of hybrid nanocomposites onto GCE was achieved via a one-step electrodeposition strategy. No less than three advantageous features are involved in the procedures of modifiers preparation, working electrode (WE) modification, and electrochemical detection. (i) the usage of precursors such as GO, nickel sulfate ($NiSO_4$), and copper sulfate ($CuSO_4$) for modifiers preparation is practically 100%, reducing the consumption of chemicals. (ii) the co-electrodeposition strategy for WE modification is essentially controllable, in-situ, rapid, and facile, averting any harsh, tedious, and time-consuming modification procedures. (iii) no hazardous organic solvents, reducing agents, mediators, and enzymes were employed during electrochemical detection, achieving a low-cost, environmental-friendly, and facile approach. The glucose sensor was used to analyse human serum sample with satisfactory results, showing potential practical application in food or pharmaceutical analysis.

2. EXPERIMENTAL

2.1 Chemicals and instrumentals

$NiSO_4$, $CuSO_4$, β-D-glucose, dopamine (DA), ascorbic acid (AA), uric acid (UA), sodium sulphate (Na_2SO_4), and sodium hydroxide (NaOH) were purchased from Sigma Aldrich. Graphite was provided by Jiangsu XFNANO Materials Tech Co., Ltd. (Nanjing, China). Nafion solution (5.0 *wt*.%) used as electrode modifier fixative was obtained from DuPont China Holding Co., Ltd. (Shanghai, China). Glucose stock solutions were prepared and diluted with distilled water (18.2 MΩ·cm) prior to use. The human serum samples were kindly offered by Hunan University of Medicine. All chemical reagents are of analytical grade and used as received without purification.

The chemical constituents, crystallization degrees, surface morphologies, and electrocatalytic properties of hybrid nanocomposites were investigated with Fourier transform infrared spectroscopy (FTIR, Thermo Scientific, Nicolet iS10, America), X-ray powder diffractometer (XRD, Rigaku, Ultima IV, Japan), Field-emission scanning electron microscopy (FESEM, Zeiss, Sigma HD, Germany), and Electrochemical workstation (EW, Shanghai Chenhua Instruments, CHI 660E, China), respectively.

2.2. Electrochemical measurements

All electrochemical measurements were carried out by the EW configured with a conventional three electrodes system under N_2 atmosphere condition and room temperature. The saturated calomel electrode (SCE), platinum wire (Diameter: 1 mm), and GCE without/with modification (Diameter: 3 mm) were acted as reference electrode, counter electrode, and WE, respectively. The electrochemical impedance spectroscopy (EIS, amplitude: 5 mV, frequency range: 0.01-100 KHz, applied potential: +0.2 V) was conducted in a mixed solution made of 0.1 M KCl and 10.0 mM $Fe(CN)_6^{3-/4-}$. Cyclic voltammetry (CV, scan rate (v): 0.1 V·s^{-1}, potential range: 0 V to +0.8 V) and amperometric current-time curve (i-t curve, sample interval: 0.1 s, quiet time: 2 s) for electrochemical glucose detection were

performed in the electrolyte solution of 0.1 M NaOH. All potentials recorded were referred to the SCE.

2.3. Preparation of modified electrodes

The rGO/Cu-Ni nanocomposites modified GCE can be one-step prepared by a controllable and in-situ electrodeposition process. Firstly, GO was obtained from graphite with the traditional Hummers method [27]. 100.0 mmol $CuSO_4$, 125.0 mmol $NiSO_4$, and 5.0 mg GO were homogeneously suspended into 5.0 mL 0.5 *wt*.% Nafion solution by ultrasonication for 20 min. Then, the surface of polished GCE was drop cast by 8.0 μL of dispersion and dried by the infrared lamp. Finally, the rGO/Cu-Ni nanocomposites formed onto GCE was achieved in deoxygenated 0.1 M Na_2SO_4 solution by performing CV in a potential range from -1.4 V to +0.2 V at a fixed v of 25 $mV{\cdot}s^{-1}$ [21]. Co-electrodeposition of precursors was terminated at successive cyclic potential scans of 16 segments. The modified electrode was rinsed with distilled water carefully and referred to as GCE|rGO/Cu-Ni. The rGO/Ni, rGO/Cu, and rGO modified GCEs were obtained by similar procedures and referred to as GCE|rGO/Ni, GCE|rGO/Cu, and GCE|rGO, respectively. The modified electrodes were stored at 4 ℃ when not in use. The procedures for modified electrode fabrication and mechanisms for electrochemical glucose detection are shown in Fig.1.

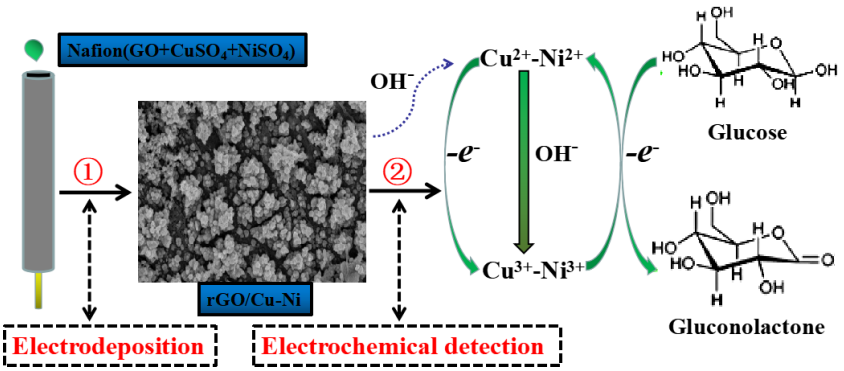

Figure 1. Schematics of rGO/Cu-Ni nanocomposites formation and electrocatalytic reactions of glucose in alkaline solution.

3. RESULTS AND DISCUSSION

3.1. Characterization of nanocomposites

Fig. 2 shows the FTIR spectra of GO, rGO, rGO/Cu, rGO/Ni, and rGO/Cu-Ni. The absorption peaks at 1380 cm^{-1}, 1230 cm^{-1}, 1060 cm^{-1}, 1620 cm^{-1}, 1720 cm^{-1}, and 3400 cm^{-1} can be ascribed to the vibrations of carboxyl C-O, epoxy C-O, alkoxy, aromatic C=C, C=O, and -OH (Fig. 2-a), showing a good agreement with the previous paper [28]. After electrochemical reduction (Fig. 2-b), the characteristic skeletal vibration relevant to aromatic C=C (1620 cm^{-1}) was persisted, while the oxygen functional groups of GO weakened significantly or disappeared, indicating that GO has been reduced

to rGO [29]. Moreover, no obvious characteristic peaks corresponding to any impurity phases can be found in the nancomposites of rGO/Cu (Fig. 2-c), rGO/Ni (Fig. 2-d), and rGO/Cu-Ni (Fig. 2-e).

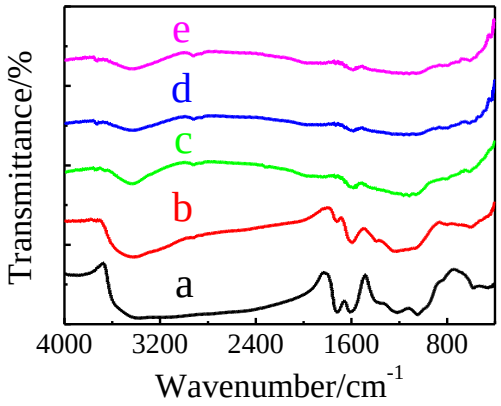

Figure 2. FTIR spectra of GO (a), rGO (b), rGO/Cu (c), rGO/Ni (d), and rGO/Cu-Ni (e).

Fig. 3 represents the XRD patterns of rGO, rGO/Cu, rGO/Ni, and rGO/Cu-Ni. The appearance of broad peak from 20° to 30° demonstrated the crystalline feature of rGO (002), indicating the rGO was formed by the electrodeposition process (Fig. 3-a) [28]. For rGO/Cu composites (Fig. 3-b), three characteristic diffraction peaks correspond to the face-centered cubic phase of Cu (220), (200), and (111) were found at 2θ=73.4°, 50.6°, and 43.4°, respectively [the standard card PDF 04-0836] [22]. The XRD pattern of rGO/Ni (Fig. 3-c) shows three typical diffraction peaks indexed to the face-centered cubic phase of Ni (220), (200), and (111) at 2θ=75.7°, 51.6°, and 44.5°, respectively [the standard card PDF 04-0850] [22]. Similar peaks were also observed in rGO/Cu-Ni (Fig. 3-d), confirming the formation of rGO/Cu-Ni nanocomposites.

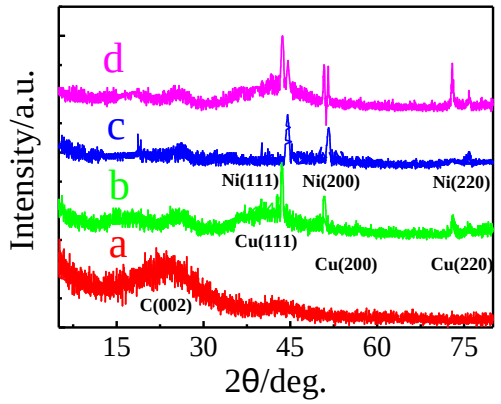

Figure 3. XRD patterns of rGO (a), rGO/Cu (b), rGO/Ni (c), and rGO/Cu-Ni (d).

Fig. 4 illustrates the surface morphologies of different electrodes. The morphology of rGO consists of some thin stacked flakes, and little irreversible agglomerates appear (Fig. 4-a). Highly dispersed Cu and Ni nanoparticles appeared on the surface of rGO (Fig. 4-b, Fig. 4-c). Upon the co-

electrodeposition, the Cu-Ni bimetallic nanocatalyst was anchored on rGO, with particle diameters of 40-80 nm (Fig. 4-d). The rGO/Cu-Ni nanocomposites formed numerous three-dimensional conducting networks, providing massive active sites for glucose electrocatalytic.

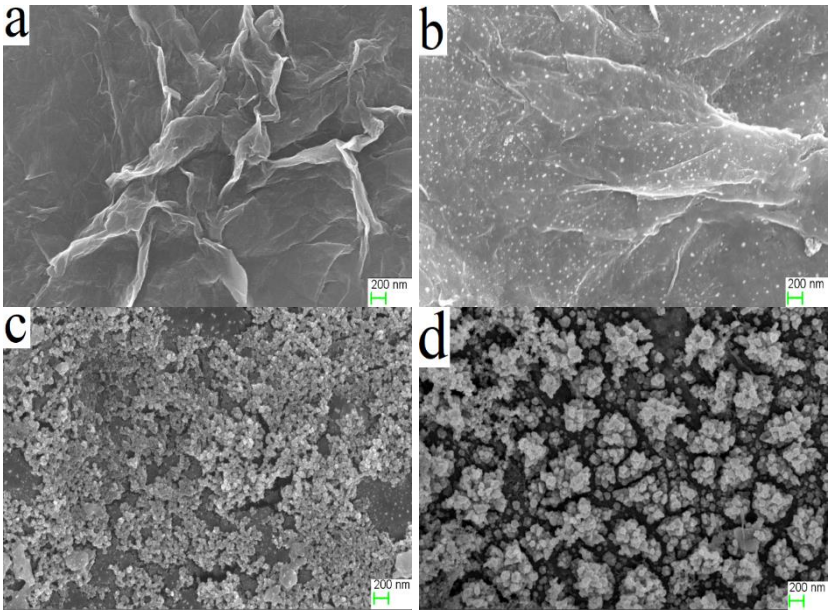

Figure 4. Surface morphologies of GCE|rGO (a), GCE|rGO/Cu (b), GCE|rGO/Ni (c), and GCE|rGO/Cu-Ni (d).

3.2. Electrochemical behaviors

The EIS consists of a line at lower frequency and a semicircle portion at higher frequency is used to characterize the interfacial changes of different electrodes (Fig. 5).

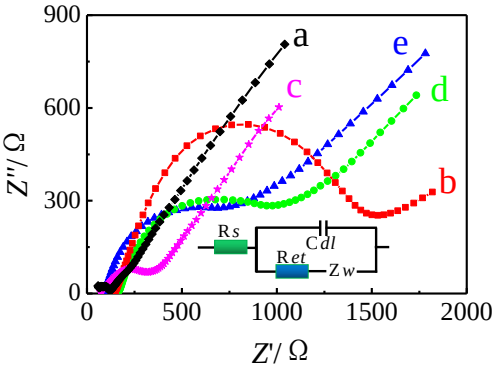

Figure 5. EISs of GCE (a), GCE|rGO (b), GCE|rGO/Cu (c), GCE|rGO/Ni (d), and GCE|rGO/Cu-Ni (e).

The randles equivalence circuit model contains the warburg impedance (Z_w), ohmic resistance of the electrolyte (R_s), double layer capacitance (C_{dl}), and electron transfer resistance (R_{et}) are used to

fit the experimental data. The semicircle portion expresses the electron-transfer limited process and the corresponding diameter equals to the R_{et}. As shown in Fig.5, the GCE showed an invisible R_{et} of 53 Ω and the minimum semicircle diameter (Fig. 5-a). The R_{et} value of GCE|rGO electrode was remarkably enhanced (1349 Ω, Fig. 5-b), attribute to the introduce of insulated Nafion that hindered the electron transfer rate of $[Fe(CN)_6]^{3-/4-}$ though rGO has excellent electrical conductivity. The values of R_{et} decreased obviously after modified by rGO/Cu (267 Ω, Fig. 5-c) and rGO/Ni (838 Ω, Fig. 5-d). When rGO/Cu-Ni was modified, the R_{et} (707 Ω, Fig. 5-e) is higher than GCE|rGO/Cu but lower than GCE|rGO/Ni. The explanation could be interpreted that the conductivity of Ni is weaker than that of Cu. The results make sure that Cu, Ni, and Cu-Ni nanoparticles can be successfully anchored on rGO.

The electrocatalytic properties of different electrodes toward glucose were investigated. No obvious glucose oxidation responses can be observed on both GCE and GCE|rGO. The GCE|rGO possess an increased background current, representing a higher active surface area of nanostructured matrix rGO. An irreversible anodic peak at +0.60 V, a pair of cathodic/anodic peaks at +0.36/+0.47 V, and a pair of cathodic/anodic peaks at +0.34/+0.49 V stemmed from the Cu^{3+}/Cu^{2+} [22], Ni^{3+}/Ni^{2+} [23], and their couples [24] were obtained from GCE|rGO/Cu, GCE|rGO/Ni, and GCE|rGO/Cu-Ni, respectively (Fig. 6). The large oxide tail obtained over +0.65 V is corresponding to the onset of water breakdown. By adding 2.0 mM glucose to the solution, the anodic peak currents increased remarkably together with the potentials shifted somewhat positively. Meanwhile, the cathodic peak currents reduced slightly without significantly changed in potentials. These results indicate that the GCE|rGO/Cu, GCE|rGO/Ni, and GCE|rGO/Cu-Ni have certain electrocatalytic oxidation activities for glucose, which has been clarified in some previous reports. The oxidation of glucose to gluconolactone can be catalyzed by both Cu^{3+}/Cu^{2+} and Ni^{3+}/Ni^{2+} redox couples according to the following reaction mechanisms (M=Cu, Ni) [22-24]:

$$M+2OH^- \longrightarrow M(OH)_2+2e^-$$

$$M(OH)_2+OH^- \longrightarrow MO(OH)+H_2O+e^-$$

$$MO(OH)+Glu \longleftrightarrow M(OH)_2+e^-+gluconolactone$$

Comparatively, the oxidation current at GCE|rGO/Cu-Ni was drastically enhanced. It is undeniable that the rGO/Cu-Ni hybrid nanointerface has synergistic effects on the catalysis of glucose. By increasing the glucose concentration to 3.0 mM, the anodic oxidation current at GCE|rGO/Cu-Ni increased. The results reveal the potential practical application of GCE|rGO/Cu-Ni in amperometric glucose detection.

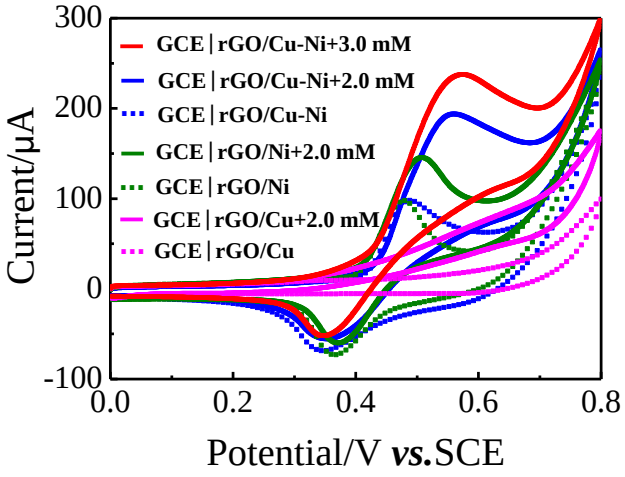

Figure 6. CVs recorded for different electrodes in absence and presence of glucose.

The effect of different *v* on oxidation of glucose at GCE|rGO/Cu-Ni was investigated by CV in 0.1 M NaOH (Fig. 7). Both cathodic peak current (Ipc) and anodic peak current (Ipa) at different *v* (100, 80, 60, 40, 20, 10 $mV \cdot s^{-1}$) are directly proportional to the *v* with two linear regression equations of Ipa(μA)=70.47 + 1.33*v* ($mV \cdot s^{-1}$) (R=0.9949) and Ipc(μA)=-6.03 - 0.57*v* ($mV \cdot s^{-1}$) (R=0.9963). The results indicate the electrochemical kinetics of glucose are surface-controlled rather than diffusion-controlled.

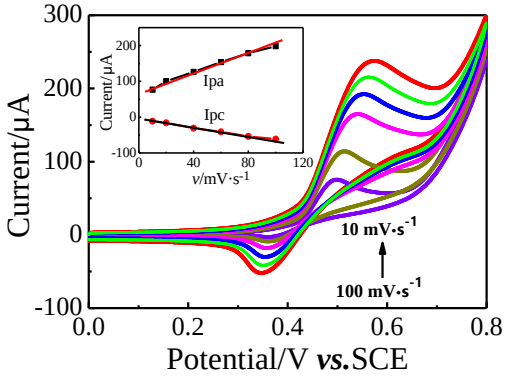

Figure 7. CVs recorded for GCE|rGO/Cu-Ni in presence of 3.0 mM glucose with different *v*.

3.3. Optimization of experimental parameters

3.3.1. Concentrations of Ni^{2+} in precursors

The electrocatalytic functions of Cu and Ni toward glucose are confirmed in Fig. 6, which implying that Ni possesses higher electroactivity and plays the dominant role during electrocatalytic oxidation of glucose.

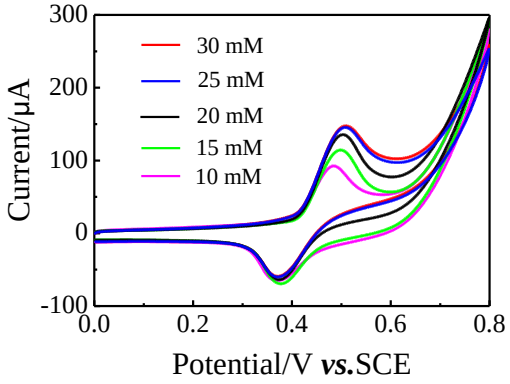

Figure 8. CVs of GCE|rGO/Ni obtained with different C_{Ni}^{2+} in presence of 2.0 mM glucose.

Therefore, it is preferential to optimize the concentrations of $NiSO_4$ (C_{Ni}^{2+}) in precursor. Five GCE|rGO/Ni were prepared by casting 8.0 μL of precursor solutions which contain 1.0 mg·mL^{-1} GO and 30 mM, 25 mM, 20 mM, 15 mM, 10 mM of Ni^{2+}, respectively. It was found that when C_{Ni}^{2+} was at a concentration of 25 mM, the most intensive oxidation current of 2.0 mM glucose can be obtained (Fig.8). The oxidation current changed little with further increased C_{Ni}^{2+}. Hence, 25 mM was chosen as the optimal C_{Ni}^{2+}.

3.3.2. Molar ratios of Cu^{2+}/Ni^{2+} in precursors

The effects of Cu^{2+}/Ni^{2+} molar ratios in precursors on catalytic performances of Cu-Ni bimetallic nanocatalyst were investigated. It is well know that the metal ions with higher redox potential are reduced earlier during co-reduction process. Notably, in terms of the Cu-Ni bimetallic nanocatalyst, the reduction of Ni^{2+} is later than that of Cu^{2+} [30, 31]. Fig. 9 show CVs of GCE|rGO/Cu-Ni towards 2.0 mM glucose with various Ni^{2+}/Cu^{2+} molar ratios (1:5, 2:5, 3:5, 4:5, and 5:5). The highest catalytic current value was obtained at 4:5 of Cu^{2+} to Ni^{2+} molar ratio, which suggests that the nanocomposites exhibit highest synergistic effects toward glucose oxidation. These results indicate that 4:5 is the optimum Cu^{2+}/Ni^{2+} molar ratio.

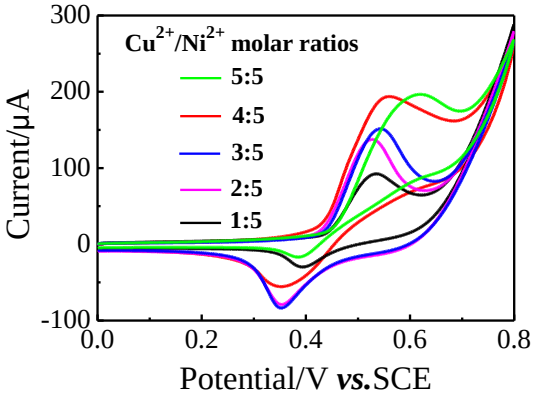

Figure 9. CVs of GCE|rGO/Cu-Ni obtained at different molar ratios of Ni^{2+}/Cu^{2+} in 0.1 M NaOH in presence of 2.0 mM glucose.

3.3.3. Potential scan numbers

The GCE|rGO/Cu-Ni obtained with different potential cycle numbers and their catalytic performances were studied by CVs in presence of 2.0 mM glucose (Fig. 10). The increases of potential cycle numbers from 4 to 16 induced the increases of glucose oxidation peak currents. The decreased oxidation peak current along with the changed peak shape were observed when the potential cycle number reached at 20. The results showed that the GCE|rGO/Cu-Ni acquired with a potential cycle number of 16 possess the biggest glucose oxidation peak current.

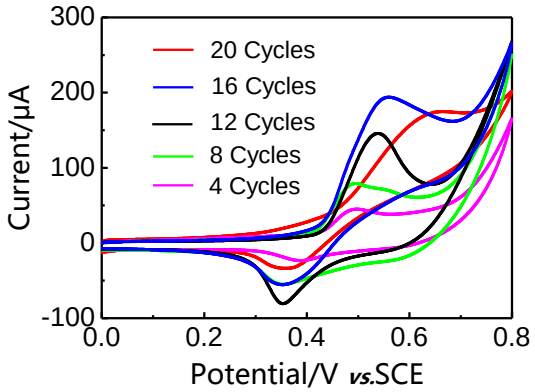

Figure 10. CVs of GCE|rGO/Cu-Ni obtained with different potential cycle number in presence of 2.0 mM glucose.

3.3.4. Detection potentials

The influences of detection potentials on amperometric responses of GCE|rGO/Cu-Ni to glucose were systematically investigated.

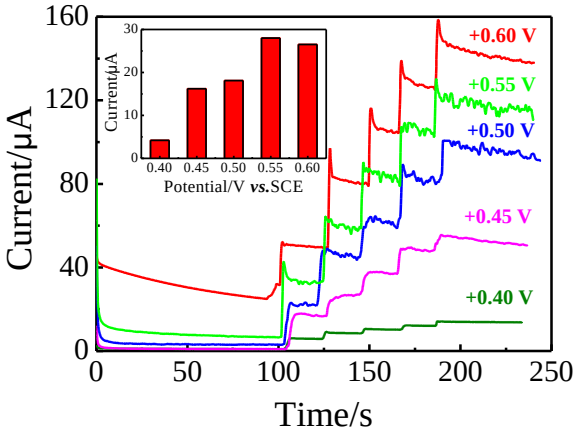

Figure 11. Current-time responses of GCE|rGO/Cu-Ni to successive additions of 0.5 mM glucose at various potentials.

The suitable detection potential was investigated by dropwise addition of 0.5 mM glucose into

0.1 M NaOH at 20 s interval under the detection potentials ranged from +0.40 V to +0.60 V (Fig. 11). A slight current response was found at potential of +0.40 V, while the biggest response current was emerged at +0.55 V. Taking the higher potentials can oxidize more intermediate interferents and unwanted species into account, +0.55 V was chosen as the detection potential to subsequently detect glucose.

3.4. Amperometric determination of glucose

Quantitative analysis of glucose was investigated with i-t curve method by recording through successive addition of glucose standard solutions into 0.1 M NaOH at the detection potential of +0.55 V (Fig. 12). The GCE|rGO/Cu-Ni generated apparent response to glucose, which coincides with the CV measurements. The enlarged amperometric current response from 0 to 140 s is inserted in Fig. 12. The steady current can be reached within 3 s towards a low concentration of glucose (4.0 μM), indicating a rapid and sensitive electrochemical response. The steady current as function of glucose concentration ($C_{glucose}$) ranged from 4.0 μM - 6.9 mM yielded a linear calibration curve with a linear equation: $I_{(\mu A)} = 1.68 + 55.33\ C_{glucose}$ (mM, R=0.9992). Based on signal: noise equals to 3:1, the limit of detection (LOD) is calculated to be 1.98 μM. Such a wide linear dynamic range (LDR) can be adapted to real sample analysis.

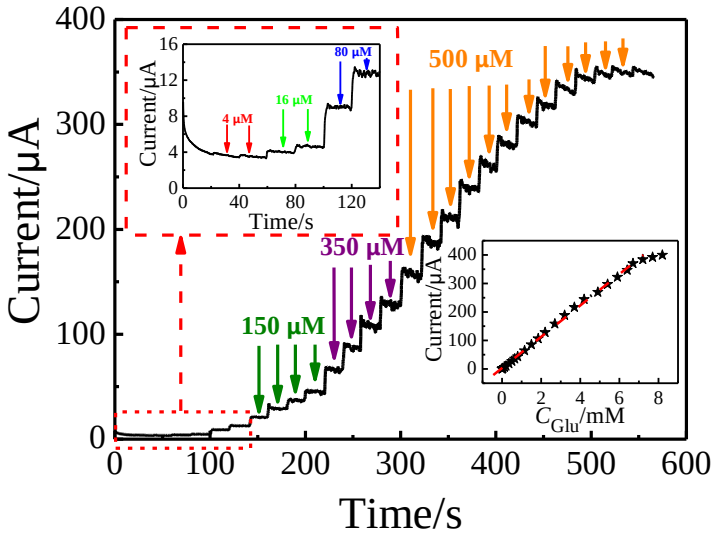

Figure 12. Typical amperometric response curve of glucose in constantly stirred electrolyte containing 0.1 M NaOH on GCE|rGO/Cu-Ni.

Table 1. Analytical performances of various nonenzymatic and enzymatic glucose sensors.

Modified electrodes	LDR(μM)	LOD(μM)	Objects	Potential(V)	Refs.
FTO[a]|CNTs-Ni/Cu	20-4500	2.0	Not given	+0.55 V *vs.*SCE	20
TiO_2 NTs[b]|Ni/Cu	10-3200	5.0	Not given	+0.6 V *vs.*Ag/AgCl	25
GCE|rGO-Ni/Co	10-2650	3.79	Serum	+0.5 V *vs.*SCE	32

GCE|CNTs-Ni	5-2000	2.0	Not given	+0.5 V *vs.*Ag/AgCl	33
MGCE[c]|Fe_3O_4-IL[d]-MWCNT@Ag/GOx	6-2000	2.12	Urine	-0.51 V *vs.*SCE	34
SPCE[e]|GNs[f]-ZnO/GOx	300-4500	70	Serum/Urine	Not given	35
GCE|rGO-MWCNT/GOx	10-6500	4.7	Urine	+0.35 V *vs.*Ag/AgCl	36
SPCE|GNR[g]-MnO_2/GOx	100-1400	50	Honey	+0.5 V *vs.*Ag/AgCl	37
GCE|rGO/Cu-Ni	4-6900	1.98	Serum	+0.55 V *vs.*SCE	This work

[a] FTO: fluorine-doped tin oxide. [b] TiO_2 NTs: TiO_2 nanotubes. [c] MGCE: magnetic glassy carbon electrode. [d] IL: ionic liquid. [e] SPCE: screen printed carbon electrode. [f] GNs: graphite nanosheets. [g] GNR: graphene nanoribbons.

The comparisons of some enzymatic and non-enzymatic glucose electrochemical sensors are summarized in Table 1. The proposed sensor shows some multiple merits including broad LDR, low LOD, and easy preparation.

3.5. Specificity, reproducibility, and stability

Some oxidizable and carbohydrate compounds including DA, AA, UA, Ur, fructose, sucrose, and lactose are commonly coexist with glucose in real samples. As far as human blood serum samples are concerned, the concentrations of glucose are significantly higher than that of interfering species (at least 30 times). The interference experiments were performed by continuously adding 0.05 mM interfering species or 0.1 mM glucose into 0.1 M NaOH with the detection potential of +0.55 V. Meanwhile, the tolerance of GCE|rGO/Cu-Ni to chloride was clarified by addition of 0.1 mM NaCl into the electrolyte. The GCE|rGO/Cu-Ni showed no significant responses to interfering species other than glucose (Fig. 13), indicating its good specificity.

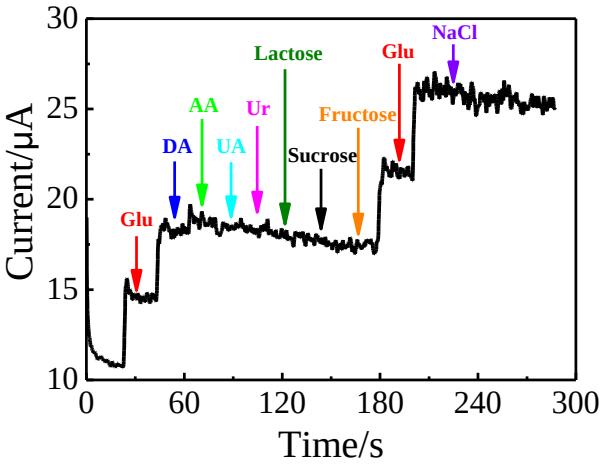

Figure 13. The i-t curve of GCE|rGO/Cu-Ni with additions of glucose and different interference substances.

The reproducibility was made upon the addition of 1.0 mM glucose into 0.1 M NaOH. The

relative standard deviations of current responses obtained by five randomly-prepared batch GCE|rGO/Cu-Ni and five successive measurements for the single GCE|rGO/Cu-Ni were 4.11% and 3.28%. Suggesting acceptable reproducibility of the modified electrode.

The stability experiments were investigated with CV under several time intervals. The results showed that the nonenzymatic sensor could be kept 97.2%, 95.8%, 93.3%, and 90.4% of the initial signal response toward 1.0 mM glucose after the modified electrode was placed in a refrigerator at 4 °C for 1 week, 2 weeks, 3 weeks, and 4 weeks. The detection signals changed by less than 10%, demonstrating the modified electrode possesses good long-time stability.

3.6. Real samples analysis

The feasible clinical applications of the nonenzymatic sensor were evaluated by determining glucose in three human blood serum samples. After centrifugal and four times dilution with 0.1 M NaOH, each sample was executed CV measurements for five times. The concentrations of glucose were calculated from the calibration curve. As revealed in Table 2, the glucose concentrations obtained with glucose sensor agree well that from the commercial Automatic Biochemical Analyzer (Hitachi 7100, Japan). Confirming great promise in practical applications.

Table 2. Results of the determination of glucose in real samples.

	Glucose sensor (n=5)		Clinical analyzer (n=5)	
Samples	Detected	*RSD*/%	Detected	*RSD*/%
1	5.84 mM	3.88	5.73 mM	3.02
2	6.21 mM	4.06	6.11 mM	2.16
3	5.77 mM	3.55	5.80 mM	2.39

4. CONCLUSIONS

An efficient nonenzymatic electrochemical sensor for glucose detection based on Cu/Ni bimetallic nanocatalyst anchored on rGO to modify GCE was fabricated. The co-electrodeposition strategy for rGO-Cu/Ni nanocomposites preparation and electrode modification is controllable, in-situ, rapid, and facile. The hybrid nanocomposites displayed superior synergistic effects toward electrocatalytic oxidation of glucose. The effectiveness was authenticated by determining real samples with satisfactory results. The universal methodologies for bimetallic nanocatalysts-based nanostructured matrices preparation and electrochemical sensing platforms fabrication offer insights for other foods and medicines detection.

ACKNOWLEDGEMENTS
This work funded by the Natural Science Foundation of Hunan Province (2021JJ40430), the Science

and Technology Innovation Program of Hunan Province (2021RC1015), the Foundation of Hunan Educational Committee (20A389), and Huaihua Science and Technology Plan Project (2021R3129, 2020R2230).

References

1. P.C. Ma, X.Y. Ma, Q. Suo and F. Chen, *Sens. Actuators B Chem.*, 292 (2019) 203.
2. V. Archana, Y. Xia, R.Y. Fang and G. G. Kumar, *ACS Sustain. Chem. Eng.*, 7 (2019) 6707.
3. H. Teymourian, A. Barfidokht and J. Wang, C*hem. Rev.*, 49 (2020) 7671.
4. W.B. Liu, X.M. Zhao, Q. Guo, Y.X. Dai, J. Tan, M.G. Wang and Y. Qi, *J. Alloys Compd.*, 895 (2022) 162573.
5. Y. Shu, T. Su, Q. Lu, Z.J. Shang, Q.Xu and X.Y. Hu, *Anal. Chem.*, 93 (2021) 16222.
6. H.X. Wu, W.M. Cao, Y. Li, G. Liu, Y. Wen, H.F. Yang and S.P. Yang, *Electrochim. Acta*, 55 (2010) 3734.
7. J. Luo, S.S. Jiang, H.Y. Zhang, J.Q. Jiang and X.Y. Liu, *Anal. Chim. Acta*, 709 (2012) 47.
8. L. Shabnam, S.N. Faisal, A.K. Roy, E. Haque, A.I. Minett and V.G. Gome, *Food Chem.*, 221 (2017) 751.
9. Y. Zhang, N. Li, Y.J. Xiang, D.B. Wang, P. Zhang, Y.Y. Wang, S. Lu, R.Q. Xu and J. Zhao, *Carbon*, 156 (2020) 506.
10. H.G Nie, Z. Yao, X.M. Zhou, Z. Yang and S.M. Huang, *Biosens. Bioelectron.*, 30 (2011) 28.
11. A.L. Sun, J.B. Zheng and Q.L.Sheng, *Electrochim. Acta*, 65 (2012) 64.
12. Y. Zhang, X.P. Xiao, Y.J. Sun, Y. Shi, H.C. Dai, P.J. Ni, J.T. Hu, Z. Li, Y.H. Song and L. Wang, *Electroanal.*, 25 (2013) 959.
13. B.K. Urhan, ÜmitDemir, T.Ö. Özer and H.Ö.Doğan, *Thin Solid Films*, 693 (2020) 137695.
14. J.X. Hao, C.L. Li, C. Wu and K.B. Wu, *Carbon*, 148 (2019) 44.
15. Z.H. Xu, Q.Z. Wang, H. Zhangsun, S. Zhao, Y.J. Zhao and L. Wang, *Food Chem.*, 349 (2021) 129202.
16. X.J. Liu, L. Long, W.X. Yang, L.L Chen and J.B Jia, *Sens. Actuators B Chem.*, 266 (2018) 853.
17. Y. Zhang, Y.Y. Ma, Y.G. Li, W.X. Zhu, Z.Y. Wei, J. Sun, T. Li and J.L. Wang, *Appl. Surf. Sci.*, 505 (2020) 144636.
18. A. Şavk, H. Aydın, K. Cellat and F. Şen, J. *Mol. Liq.*, 300 (2020) 112355.
19. K.C. Lin, Y.C. Lin and S.M. Chen, *Electrochim. Acta*, 96 (2013) 164.
20. S. Ammara, S. Shamaila, N. Zafar, A. Bokhari and A. Sabah, *J. Phys. Chem. Solids*, 120 (2018) 12.
21. C.L. Zhang, F.S Li, S.Q Huang, M.T Li, T.Y. Guo, C.H. Mo, X. Pang, L.M. Chen and X.C. Li, *J. Colloid Interface Sci.*, 557 (2019) 825.
22. W. Yi, J. Liu, H.B. Chen, Y. Gao and H.M. Li, *J. Solid State Electrochem.*, 19(2015) 1511.
23. L. Shabnam, S.N. Faisal, A.K. Roy, A. I. Minett and V. G. Gomes, *Electrochim. Acta*, 224 (2017) 295.
24. K.L. Wu, Y.M. Cai, B.B. Jiang, W.C. Cheong, X.W. Wei, W.Z. Wang and N. Yu, *RSC Adv.*, 7 (2017) 21128.
25. X.L. Li, J.Y. Yao, F.L. Liu, H.C. He, M. Zhou, N. Mao, P. Xiao and Y.H. Zhang, *Sens. Actuators B Chem.*, 181 (2013) 501.
26. D.D. Cui, L. Su, H.J. Li, M.J. Li, C.P. Li, S. Xu, L.R. Qian and B.H. Yang, *J. Electroanal. Chem.*, 838 (2019) 154.
27. X. Yang, F.B. Xiao, H.W. Lin, F. Wu, D.Z. Chen and Z.Y. Wu, *Electrochim. Acta*, 109 (2013) 750.
28. X. Yang, Q.J. Guo, J.H. Yang, S.L. Chen, F.L. Hu, Y.J. Hu and H.W. Lin, *Food Chem.*, 338 (2021) 127851.
29. X. Yang, Y.J. Ouyang, F. Wu, Y.J. Hu, Y. Ji and Z.Y. Wu, *Sens. Actuators B Chem.*, 238 (2017) 40.

30. W.Z. Li, L. Kuai, Q. Qin and B.Y. Geng, *J. Mater. Chem. A*, 1 (2013) 7111.
31. L. Zhang, C. Ye, X. Li, Y.R. Ding, H.B. Liang, G.Y. Zhao and Y. Wang, *Nano-Micro Lett.*, 10 (2018) 28.
32. L. Wang, X.P. Lu, Y.J. Ye, L.L. Sun and Y.H. Song, *Electrochim. Acta*, 114 (2013) 484.
33. T.J. Choi, S.H. Kim, C.W. Lee, H. Kim, S.K. Choi, S.H. Kim, E.K. Kim, J. Park and H.J. Kim, *Biosens. Bioelectron.*, 63 (2015) 325.
34. M. Baghayeri, H. Veisi and M. Ghanei-Motlagh, *Sens. Actuators B Chem.*, 249 (2017) 321.
35. C. Karuppiah, S.K. Palanisamy, S.M. Chen, V. Veeramani and P. Periakaruppan, *Microchim Acta*, 181 (2014) 1843.
36. V. Mani, B. Devadas and S.M. Chen, *Biosens. Bioelectron.*, 41 (2013) 309.
37. V. Vukojević, S. Djurdjić, M. Ognjanović, M. Fabian, A. Samphao, K. Kalcher and D. M. Stanković, *J. Electroanal. Chem.*, 823 (2018) 610.